ACS Partner Journal

Journal of the American Society for Mass Spectrometry

pubs.acs.org/jasms

Research Article

Pneumatically Sprayed Gold Nanoparticles for Mass Spectrometry Imaging of Neurotransmitters

Nolan McLaughlin, Tyler M. Bielinski, Caitlin M. Tressler, Eric Barton, Kristine Glunde, and Katherine A. Stumpo*

Cite This: *J. Am. Soc. Mass Spectrom.* 2020, 31, 2452–2461

Read Online

ACCESS | Metrics & More | Article Recommendations | Supporting Information

ABSTRACT: Using citrate-capped gold nanoparticles (AuNPs) for laser desorption ionization mass spectrometry (LDI-MS) is an approach that has demonstrated broad applicability to ionization of different classes of molecules. Here, we show a simple AuNP-based approach for the ionization of neurotransmitters. Specifically, the detection of acetylcholine, dopamine, epinephrine, glutamine, 4-aminobutyric acid, norepinephrine, octopamine, and serotonin was achieved at physiologically relevant concentrations in serum and homogenized tissue. Additionally, pneumatic spraying of AuNPs onto tissue sections facilitated mass spectrometry imaging (MSI) of rabbit brain tissue sections, zebrafish embryos, and neuroblastoma cells for several neurotransmitters simultaneously using this quick and simple sample preparation. AuNP LDI-MS achieved mapping of neurotransmitters in fine structures of zebrafish embryos and neuroblastoma cells at a lateral spatial resolution of 5 μm. The use of AuNPs to ionize small aminergic neurotransmitters in situ provides a fast, high-spatial resolution method for simultaneous detection of a class of molecules that typically evade comprehensive detection with traditional matrixes.

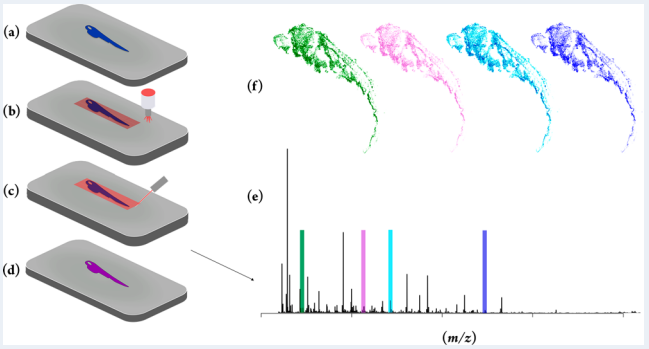

KEYWORDS: *mass spectrometry imaging, neurotransmitters, gold nanoparticles, zebrafish, neuroblastoma*

INTRODUCTION

Advancements in mass spectrometry (MS) over the past 100 years can be traced through publication trends[1] and range from fundamental small molecule ion chemistry to new discoveries in ionization that allow for the comprehensive analysis of biomolecules, including proteomics,[2−4] lipidomics,[5−7] and perhaps most recently, metabolomics.[8−11] Untargeted analysis, aided concomitantly by the incorporation of data science to MS, has emerged as one of the most powerful tools in the postgenomics era.[12,13] The quality and quantity of the obtained MS raw data (i.e., the number and intensity of peaks generated) strongly depends on the ionization process itself. Traditional organic matrixes (e.g., α-cyano-4-hydroxycinnamic acid (CHCA), 2,5-dihydroxybenzoic acid (DHB), and 5-dimethoxy-4-hydroxycinnamic acid, also known as sinapic or sinapinic acid (SA)) have found widespread use in matrix-assisted laser desorption/ionization (MALDI)-MS of various biomolecules,[14] including lipids, proteins, and carbohydrates, but have struggled to enable the ionization of small molecules.[15] Small molecule detection has improved with the introduction of *N*-(1-naphthyl) ethylenediamine dihydrochloride (NEDC) and 1,5-diaminonaphthalene (DAN). Ultimately, with the large number of choices available, detailed knowledge of what matrix will ionize which biomolecular class is needed. In contrast, we propose the use of gold nanoparticles (AuNPs), which thus far have broad applicability across biomolecule classes, including carbohydrates, amino acids, peptides, neutral steroids, and others,[16,17] and have particularly unique ionization capabilities for small molecules.

Mass spectrometry imaging (MSI) is a powerful molecular imaging tool that provides highly multiplexed molecular information using a label free method. While the use of MALDI-MSI is gaining traction in basic science and biomedical applications,[18−22] it is still faced with significant challenges in (i) sample preparation and (ii) the effective lateral spatial resolution that can be achieved. More specifically, maintaining optimum conditions for homogeneous matrix crystal formation can be a challenge in MALDI imaging. While the introduction of pneumatic sprayers[23−25] and sublimation procedures[26−28] have dramatically reduced this limitation, there is still a fundamental limit on crystal size and therefore pixel size.[29] Additionally, analyte delocalization is a

Special Issue: Focus: 2019 Asilomar Meeting - MS Imaging

Received: April 30, 2020
Revised: August 25, 2020
Accepted: August 25, 2020
Published: August 25, 2020

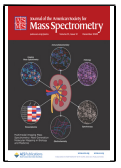

continuing challenge to mitigate;[30,31] the matrix needs to extract analyte molecules as well as maintain sample integrity even for analytes with high diffusivity. Instrument-to-instrument and lab-to-lab reproducibility is still an issue in MSI,[32] specifically with regards to sample preparation. Lateral spatial resolution in commercial instruments ranges from 5 to 20 μm[33,34] with other reports of home-built instruments going as low as 600 nm.[35−37]

Neurotransmitters (NTs) have been difficult to detect in situ using traditional MALDI techniques due to their low abundance (e.g., nanomolar to picomolar concentrations) and low molecular mass, resulting in a high chemical noise and m/z overlap with most traditional matrixes. The only previous MSI experiments that have succeeded with highly multiplexed detection of NTs in tissue have used chemical derivatization methods.[38,39] The additional steps and time required for derivatization affect the ability to achieve true high throughput (HTP) and may increase the chances of analyte delocalization.[40,41] Previous reports of NT MSI also required different (or multiple) matrix preparations in order to effectively detect NTs that are not primary amines (e.g., ACh and α-GPC).[38]

Inorganic materials, i.e., nanoparticles (NPs), have been widely utilized in MS and have unique effects on ionization that are not observed with traditional organic matrixes yet have not been met with mainstream usage. Materials have included gold,[16,17,42−45] silver,[46,47] silicon,[48] and carbon.[49−51] Specifically, AuNPs have been shown to ionize peptides,[17,52] bile acids,[16,42] carbohydrates,[16,42,44] steroids,[16,43] and other lipids.[42,47,53,54] Multiple applications of AuNPs with various analyte interactions have been published.[55] Demonstrations of AuNP-enhanced imaging of tissues[56] or plant materials[57] have resulted in lateral spatial resolutions of 100 μm. Sputtering of NP nanolayers onto tissue or plant sections have enabled imaging of biomolecules; however, sputtering NPs has challenges with consistent NP size and the availability of the necessary equipment.[58−61] The ionization mechanism of NPs is not fully understood,[16,17,42,53] though prior studies suggest that energy transfer from AuNPs to the analyte may occur through a thermally driven mechanism; this lack of consensus may contribute to the sporadic usage of these types of materials.

Here, we describe the ionization of individual NTs and of endogenous NTs from biological samples using citrate-capped AuNPs. We introduce MSI using pneumatically sprayed AuNPs on tissue sections, which overcomes several frequently cited issues in MSI and presents a reduced time and cost alternative to current methods for small molecule analysis. Specifically, we address delocalization, reproducibility (shot-to-shot and repeated runs), long-term stability of readily prepared tissue sample, and ionization efficiency of NTs and other small molecules.[62,63]

METHODS

Materials. The following were purchased from Millipore-Sigma (St. Louis, MO): α-cyano-4-hydroxycinnamic acid (CHCA), acetonitrile, acetylcholine chloride, ammonium bicarbonate, 2,5-dihydroxybenzoic acid (DHB), dopamine hydrochloride, epinephrine hydrochloride, γ-aminobutyric acid, glutamic acid monosodium salt, norepinephrine bitartrate, octopamine hydrochloride, poly-D-lysine, serotonin hydrochloride, sinapinic acid (SA), tricaine methanesulfonate, and HPLC grade water and methanol. All reagents were ACS grade or higher, unless noted. Gold nanoparticles (AuNPs) with nominal sizes of 2 and 5 nm were purchased from Ted Pella, Inc. (Redding, CA). Sterile-filtered human serum was purchased from Sigma-Aldrich (St. Louis, MO). Young frozen rabbit brains stripped of meninges were purchased from Pel-Freeze (Rogers, AK). There were no additional safety considerations outside of normal chemical hygiene procedures.

Crayfish Brain Preparation. Previously dissected and frozen crayfish brains (*Procambarus clarkii*) from Carolina Biological Supply (Burlington, NC) were thawed to room temperature and were mixed with 250 μL of pH 7.0 buffered 25 mM ammonium bicarbonate (ABC) and manually homogenized using a mortar and pestle. Next, another 250 μL of ABC was added and the sample split and was transferred to two test tubes that were spun at 8000 rpm for 8 min in a 3000 MWCO spin filter (EMD Millipore, Burlington, MA). The flow through was retained and spun again at 8000 rpm for 10 min and then 14 000 rpm for 5 min. The remaining solution was distributed into 100 μL tubes, and AuNPs was added; the empirically determined optimum AuNP-to-analyte ratio was for 5 μL of 2 nm AuNPs to be added to 100 μL of sample.

Zebrafish Husbandry. Adult zebrafish (*Danio rerio*) were purchased from Carolina Biological Supply (Burlington, NC) and bred, and embryos were collected. Within 4 h of postfertilization, embryos were transferred to Petri dishes containing embryo medium (E3) and kept at 28 °C. E3 buffer was changed daily until 5 days of postfertilization when embryos were sacrificed using a 600 mg/L solution of tricaine methanesulfonate. All animal handling procedures were approved by IACUC #9-19 at the University of Scranton.

Neuroblastoma Preparation. Neuroblastoma cells (SK-N-SH, HTB-11) were purchased from ATCC (Manassas, VA) and kept frozen until use. Cells were cultured in Dulbelco's modified eagle medium in a glass Petri dish and across cleaned indium tin oxide (ITO) slides (Delta Technologies, Loveland, CO) coated with poly-D-lysine. Neuroblastoma cells were placed in a desiccator for 5 min before spraying with AuNPs (spraying details below).

Sample Preparation. Aqueous NT solutions were prepared at 1 mg/100 μL. Using 2 and 5 nm AuNPs individually, samples had a final ratio of 1 AuNP/10^5 analyte molecules; samples were plated using the dried droplet method. Traditional matrixes of CHCA, DHB, and SA were mixed with analyte molecules at a ratio of 10^5 matrix/1 analyte and spotted on target plates using the dried droplet method. Human serum samples were prepared at a concentration of 1 mg/10 μL, and an appropriate ratio of AuNPs was placed into solution. NT spiked organic matrix samples were prepared by taking the same starting serum sample, through adding 5 μL of a previously prepared NT solution (including matrix) and plating using the dried droplet method.

LDI and MALDI-MS Analysis. All target-plate-based experiments were performed on a Kratos Axima MALDI-TOF MS (Shimadzu Scientific Instruments, Columbia, MD). Conditions were optimized in positive ion reflectron mode, using pulsed extraction with a N_2 laser at 337 nm. Similar instrument conditions were used for traditional matrix and AuNP experiments. In general, an increase in laser power is needed for the AuNP samples compared to traditional matrixes, with little difference in power for 2 and 5 nm AuNPs. Target-plate-based experiments were repeated for efficacy on a Bruker Rapiflex MALDI TOF/TOF mass spectrometer (Bruker Daltonics Instruments, Billerica, MA) in reflectron positive ion mode with a Nd:YAG laser at 355

https://dx.doi.org/10.1021/jasms.0c00156
J. Am. Soc. Mass Spectrom. 2020, 31, 2452−2461

nm. Since the data obtained were similar to previous target plate experiments on the Shimadzu Axima, no target plate data from this instrument are shown here. Note, this is the first demonstration across instruments (i.e., lasers) for this method. MS/MS experiments were done on a Bruker Rapiflex MALDI TOF/TOF instrument in profiling mode using an M5 flat laser with 114 μm resultant field with 4000 laser shots and argon gas collision induced dissociation (CID). All measurements were completed with a ± 1 Da isolation window. Measurements were performed on tissue from the head region of the zebrafish embryo. MS/MS spectra of pure NTs were measured on a stainless steel target plate using the same method.

Mass Spectrometry Imaging. Zebrafish embryos were placed in a 10 mm × 10 mm × 5 mm biopsy cryomold (Ted Pella) and embedded in Thermo Scientific Shandon M1 embedding media (Thermo Fisher Scientific, Waltham, MA). After freezing, the block was sectioned at 10 μm thickness at −16 °C and thaw-mounted onto cleaned ITO slides. Fresh frozen rabbit brain was sectioned at −20 °C without embedding in media at 10 μm thickness and thaw-mounted onto cleaned ITO slides. All cryo-sectioning was done on a Leica CM1860 cryostat (Buffalo Grove, IL). A traditional organic matrix preparation was performed using 10 mg/mL DHB in 50% MeOH/50% water and sprayed using an HTX M5 sprayer (HTX Technologies LLC, Chapel Hill, NC) with a nozzle temperature of 85 °C. Eight passes were sprayed at a flow rate of 0.075 mL/min with no drying time. Using the HTX M5 sprayer, 2 nm AuNPs were sprayed at either 30 or 45 °C. One pass was sprayed at a flow rate of 0.010 mL/min with 2 s drying time. All imaging experiments were performed on Bruker Rapiflex MALDI-TOF/TOF mass spectrometer. Spectra were obtained in positive ion mode with 200 laser shots per pixel.

Data Processing. All data was converted to imzML using flexImaging version 5.0 (Bruker Daltonics). The imzML files were then converted in msiQuant[64] for analysis and processing. RStudio was also used for data analysis. The package Cardinal[65] under the Bioconductor Normalization was performed using a total-ion-count (TIC) method. Regions of interest were selected by hand.

RESULTS/DISCUSSION

NTs analyzed here include acetylcholine (ACh), dopamine (DA), epinephrine (EP), 4-amino butyric acid (GABA), glutamine (GLU), norepinephrine (NE), octopamine (OT), and serotonin (5-HT). Supporting Information Table S1 details the species observed for individual NTs using 2 and 5 nm AuNPs, along with Figures S1−S7 showing mass spectra for all NTs listed. Interestingly, ACh on the target plate did not require AuNPs to ionize (attributed to the quaternary amine with permanent charge, see Figure S1) but did on tissue. While these control experiments were done to determine if any NTs desorb as preformed ions, differences between the target plate and on tissue were expected. We infer that differences in analyte concentration and the overall complexity of the background matrix affected ionization efficiency. Additionally, salt adducts were present, with fewer being observed for 5 nm as compared to 2 nm AuNPs; salt adducts are expected due to the high concentration of Na^+ and K^+ from the AuNP solution. All pure compounds tested using AuNPs resulted in a reduction in background chemical noise as compared to organic matrixes, which aided the detection of the NTs. Detection of NTs with AuNPs was compared to that with all-purpose organic matrixes (i.e., DHB or CHCA, see Figure S8), which were unable to provide conclusive results for many of the NTs. Specifically, the use of DHB resulted in overlapping analyte peaks and matrix background chemical noise (e.g., 5-HT, DA, EP, GLU, and OT), i.e., analyte and matrix peaks could not be distinguished because of multiple isobaric species.

To show the efficacy of AuNPs to ionize NTs from a complex mixture, we analyzed homogenized crayfish brains. This is a particularly difficult sample to analyze using MS due to the small chemical footprint of the target molecules. AuNPs ionized many of the NTs typically found in a crayfish brain. Specifically, 2 nm AuNPs ionized DA/OT, EP, NE, 5-HT, ACh, GLU, and GABA/choline (see Figure 1a) and 5 nm

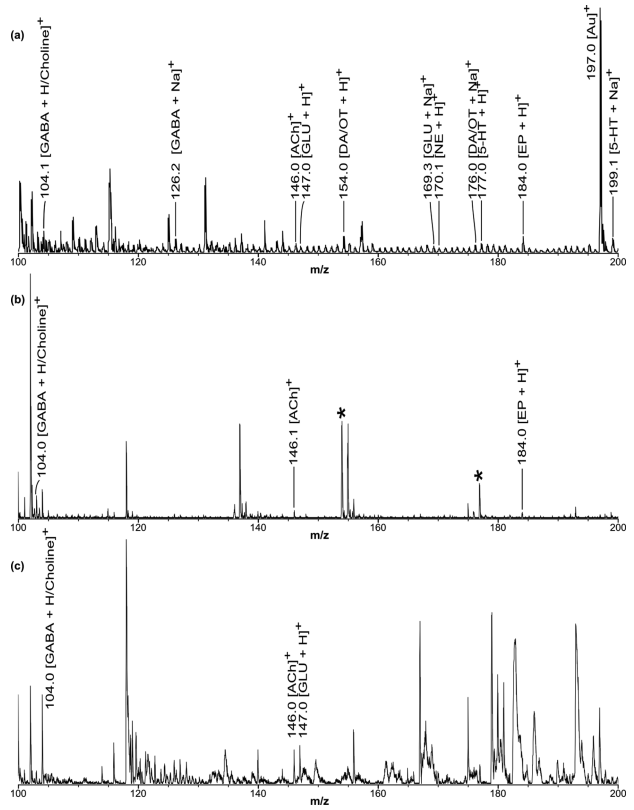

Figure 1. Positive ion LDI mass spectra of homogenized crayfish brain using (a) 2 nm AuNPs with an intensity of 680 mV, (b) SA with an intensity of 1382 mV, and (c) DHB with intensity of 144 mV. All detected NTs are labeled as well as the Au^+ ion. These data were collected on a Shimadzu Axima.

AuNPs ionized ACh, DA/OT, EP, GABA/choline, and GLU, 5-HT. Compared to analysis with DHB (Figure 1b), more NTs were observed with AuNPs and there was no overlap of matrix with potential NT signals (labeled as *); additionally, the optimized instrument conditions yielded a higher ion detection of 680 mV for AuNP compared to 144 mV with DHB. Analysis with SA (Figure 1c) resulted in very high baseline noise that arises from needing a higher laser power to observe any signal at all, and therefore, overall ion detection was 1382 mV but with only two NTs observed. Chemical background noise is still present with AuNPs but is improved from organic acid matrixes. Traditional methods of analysis for NTs in crayfish (and other vertebrate systems) typically include high-performance liquid chromatography-electrochemical detection (HPLC-ECD), which can be time-consuming

https://dx.doi.org/10.1021/jasms.0c00156
J. Am. Soc. Mass Spectrom. 2020, 31, 2452−2461

and requires significant method development.[66] This novel application of AuNPs could potentially transform the ability to analyze NTs in tissue homogenates of a variety of organisms commonly used in neuroscience research.

To further assess the utility of AuNPs for NT detection in biological samples, human serum was analyzed. Both 2 and 5 nm AuNPs ionized NTs at circulating physiological concentrations, for which many of the NT concentrations are in the 100s of pg/mg.[67,68] Figure 2 shows 2 nm AuNPs ionizing

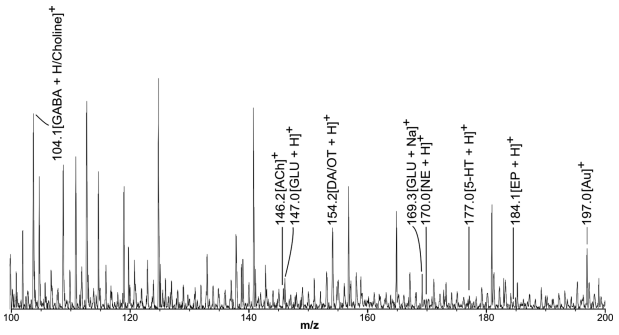

Figure 2. Positive ion LDI mass spectrum of human serum using 2 nm AuNPs. All detected NTs are labeled as well as the Au^+ ion.

GABA/choline, GLU, DA/OT, 5-HT, NE, and EP. This is the first known example of AuNPs ionizing NTs at a physiologically relevant concentration (e.g., the typical circulating concentration of DA in serum of 200 pg/mL).[67,68] As an additional comparison, SA, CHCA, and DHB were run with spiked NTs in order to assess ionization suppression. All organic matrix spectra had significant chemical noise in the low mass region (see Figure S9).

Although DHB may have produced signals for DA/OT and 5-HT, it was not possible to distinguish these from matrix peaks. Also, to generate significant signal intensities for CHCA, a high laser power was required, resulting in more spectral noise and poor spectral resolution. DHB also failed to ionize EP and GLU. CHCA did not ionize DA, EP, OT, and 5-HT. In contrast to organic matrixes, both 2 and 5 nm AuNPs were able to ionize all NTs, highlighting the importance of matrix choice in LDI-MS when working in the mass range below m/z 300. Limits of detection (LODs) were determined on the target plate, and concentrations as low as femtomole/microliter per spot were ionized using 2 and 5 nm AuNPs for all analytes. All resulting spectra were comparable within 2 orders of magnitude of analyte concentration and within 2 orders of magnitude of AuNP/analyte, as previously discussed[16,17] (see the Methods section for details). Few previous LOD determinations of NTs have been done using LDI-MS. The closest comparisons for LDI-MS were an analysis of DA in the nanogram/milliliter range[69] and another study detecting NE and EP in the nanomole/gram range from tissue.[70] Additionally, electrospray ionization of select NTs has been reported in the nanomolar range (of 5-HT, DA, and their metabolites)[71] and in the nanogram range (of 5-HT, DA, and their metabolites).[72]

Next, we tested the applicability of AuNPs for LDI-MSI and examined coronal rabbit brain tissue sections (10 μm thickness) as a proof-of-concept experiment. Given the similarity in performance of 5 and 2 nm AuNPs on the target plate, only 2 nm AuNPs were used from this point forward. The same NTs that were detected in target plate experiments were also observed in LDI-MSI; Figure 3a shows the optical image of the rabbit brain section for reference, and Figure 3b–

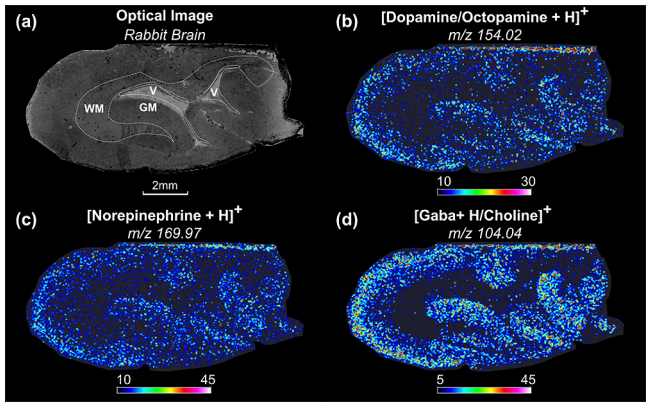

Figure 3. MSI of coronal rabbit brain tissue section at 20 μm lateral spatial resolution: (a) optical image with annotations for white matter (WM), gray matter (GM), and ventricles (V), (b) DA/OT image at m/z 154.02, (c) NE image at m/z 169.97, and (d) GABA/choline image at m/z 104.04.

d shows the distribution of DA/OT, NE, and GABA/choline at 20 μm lateral spatial resolution. Importantly, the images show a difference between white and gray matter regions of the brain, with the visualization of the folds of the gray matter and the interior cavity of white matter that typically lacks NT signal. White matter contains axons, which are typically surrounded by the myelin sheath; gray matter contains most of the neuronal cell bodies, leading to an expected difference in NT abundance. GABA,[73,74] DA,[75] and NE[75] have previously been shown to have differences in concentration in white vs gray matter using magnetic resonance imaging techniques, though this has not previously been visualized using MSI. The ability to map NT location is useful for neurological research; for example, DA detection in white matter has been used for tracking the progression of disease in Huntington's[76] and Parkinson's diseases,[77,78] and gray matter density informs on fibromyalgia.[79] Finally, tissue sections, which contain fewer salt adducts than target plate experiments, resulted in images showing much lower intensity in Na^+ and K^+ adducts of NTs than those observed in target plate experiments (see Supporting Information Figure S10). This could be attributed to a change in how ionization occurs, with the soft desorption of protonated species being more favorable than that of the salt adduct; more experimentation to evaluate these differences is needed and ongoing.

The mass spectrum for rabbit brain slices, which was normalized to total ion count (TIC), is shown in Figure 4 with a comparison to tissue sprayed with CHCA. In Figure 4a near m/z 104 and 184, there is baseline distortion and there is an area where no additional peaks are observed, which could result from the high intensity of these two peaks. CHCA is known to extract lipids, and m/z 184 is typically identified as the phosphatidylcholine headgroup or cytosolic phosphocholine, which also results in m/z 104 as choline as a decomposition product or free choline present in the cytosol.[80,81] For the AuNP samples, MS/MS of pure GABA and choline do not show any fragmentation differences and m/z 184 is confirmed as NE (see Supporting Informtion Figure S11). Even with minimal spraying of organic matrix, the tissue is saturated with these two ions, resulting in few identifiable

https://dx.doi.org/10.1021/jasms.0c00156
J. Am. Soc. Mass Spectrom. 2020, 31, 2452−2461

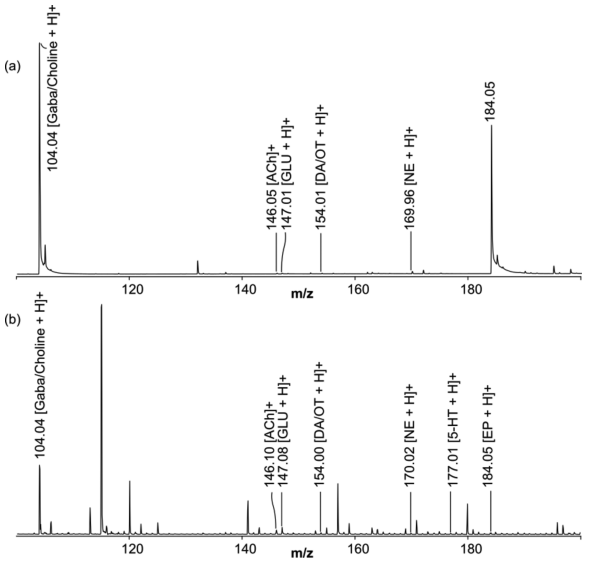

Figure 4. Positive ion LDI mass spectra of 10 μm sliced rabbit brain tissue section, normalized to TIC: (a) CHCA spectrum with an intensity of 825 au and (b) 2 nm AuNP spectrum with an intensity of 6.55 au. All detected NTs are labeled. These data were collected on a Bruker Rapiflex.

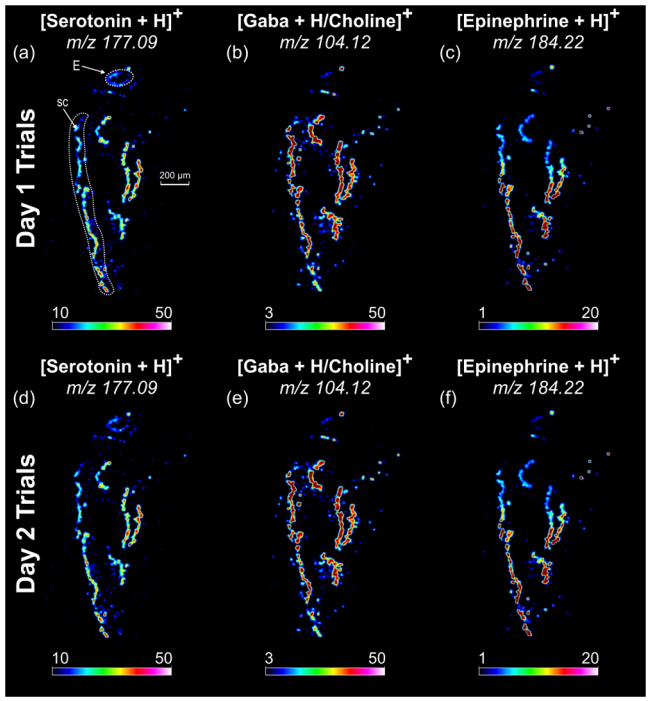

Figure 5. MSI of axial zebrafish embryo tissue section at 20 μm lateral spatial resolution: (a and d) GABA/choline images at m/z 104.12, (b and e) 5-HT images at m/z 177.09, and (c and f) EP images at m/z 181.05. The top row of images was acquired directly after spraying of AuNPs onto tissue. The bottom row of images was a second imaging run of the same tissue section acquired after overnight storage in a −20 °C freezer and without spraying new AuNPs.

peaks in the low-mass range. Overall, AuNPs are advantageous for sample preparation and preservation of signal intensities. An additional improvement of using AuNPs for MSI is that there is minimal to no delocalization of the analyte. Supporting Information Figure S12 shows a typical CHCA spraying protocol on a rabbit brain tissue section and the resulting delocalization, where m/z signals extend beyond the tissue margins (bold white line).

Expanding the utility of MSI to zebrafish embryos, which are 1−2 mm in size, presents several new challenges, including tissue preparation (e.g., mounting and cryo-sectioning) and if MSI can be achieved at a high enough spatial resolution to adequately map the distribution of NTs. This organism is of interest because it is a widely accepted model for genetic[78,82] and neuroscience[83,84] studies owing to its similarities in neuroanatomy and development to higher level vertebrates,[85,86] as well as conservation of metabolic pathways.[87] Finally, the rapid breeding cycle, basic husbandry, and early morphology make zebrafish an attractive model. Figure 5 shows the MSI data from 10 μm thick tissue sections of 5 day postfertilization (dpf) zebrafish embryos imaged at 20 μm lateral resolution from an axial cryo-sectioning orientation, with spraying of only one pass of AuNPs for sample preparation. All the previously characterized NTs were observed by MSI, with images of 5-HT, GABA/choline, and epinephrine shown in Figure 5 (with embryo orientation of eye at the top and tail at the bottom). The neural tube (i.e., spinal cord) contains neural crest cells that migrate concomitantly with somites, followed by subsequent somite differentiation into the basal lamina;[88] this allows for observation of the outline of the rapidly expanding somatic muscle that surrounds the spinal cord and notochord. Figure 5d−f (bottom row) shows a subsequent imaging run performed on the tissue after storing the slide overnight at −20 °C. There is no apparent difference in the NT spatial images after freezing the tissue, and no additional application of AuNPs was required. The ability to acquire additional data on tissue allows for repeated runs and could significantly impact methods of data collection and the number of organisms required in research. Additional imaging runs (up to 8) were performed on multiple tissue areas, and there was no discernible difference in the spatial distribution of NTs and intensity after repeated laser shots on the same area. Supporting Information Figure S13 shows the average mass spectrum from the first and second imaging runs. Organic matrixes typically require exacting conditions in order to effectively image small molecules and do not allow for repeat runs without washing and matrix reapplication,[89−91] yet we have demonstrated that there is extreme flexibility in storage of tissue when using AuNPs for MSI. For confirmation of the detected NT species in zebrafish, we used anatomical clues from a tissue atlas,[92] computational data analysis methods (e.g., segmentation analysis), and MS/MS (see Supporting Information Figures S11 and S14−S21). We are conducting further experiments to determine the full range of sample flexibility; for example, thus far 10 precursor ions have been verified using MS/MS on one zebrafish tissue section with no loss of signal, suggesting that more are possible. To the best of our knowledge, these are the first MSI data of zebrafish embryos that simultaneously map multiple NTs, which presents exciting new opportunities for developmental biology research. The corresponding skyline mass spectrum from the MSI run is shown in Figure S22. Note that the skyline spectrum is shown so that low-intensity ions will have the same intensity as they appear at the individual pixel level even though they may only be present in a small fraction of the pixel spectra. The skyline spectrum was used so that a maximum number of signals could be interrogated to detect other small

https://dx.doi.org/10.1021/jasms.0c00156
J. Am. Soc. Mass Spectrom. 2020, 31, 2452−2461

molecules of interest, possibly beyond neurotransmitters. A fully detailed examination of these data is ongoing.

In addition to these proof-of-concept experiments on various biological samples and tissues, we have pushed the limits of lateral spatial resolution on tissue using AuNPs for LDI-MSI of zebrafish embryos. Figure 6 shows LDI imaging at 5 μm spatial

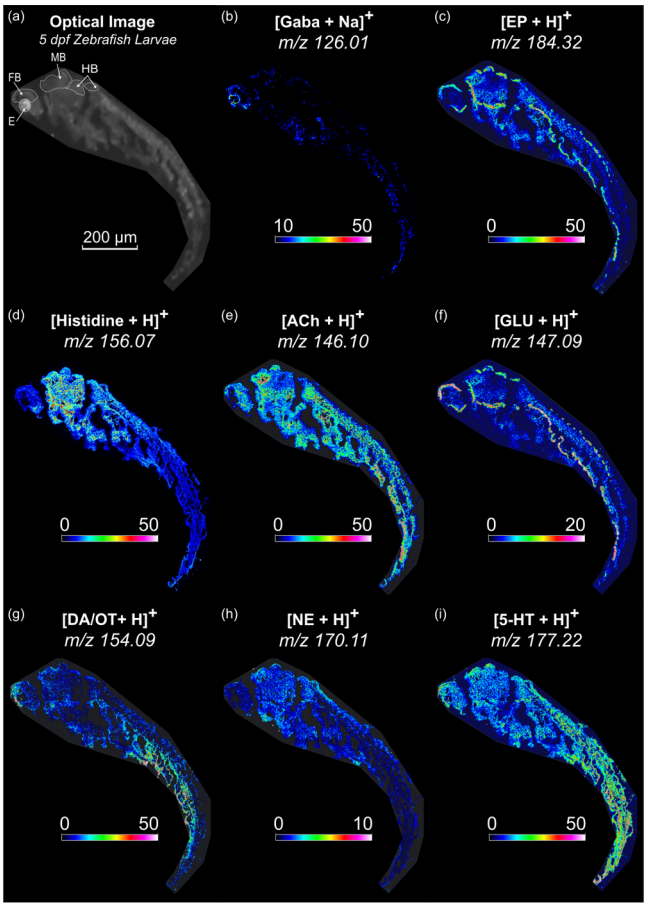

Figure 6. MSI of a sagittal zebrafish tissue section at 5 μm lateral spatial resolution: (a) optical image with eye (E), forebrain (FB), midbrain (MB), and hindbrain (HB) indicated, (b) GABA + Na^+ image at m/z 126.01, (c) EP image at m/z 184.32, (d) histidine image at m/z 156.07, (e) ACh image at m/z 146.10, (f) GLU image at m/z 147.09, (g) DA/OT image at m/z 154.09, (h) NE image at m/z 170.11, and (i) 5-HT image at m/z 177.22.

resolution of sagittally cryo-sectioned 5 dpf zebrafish embryos. The scanned optical image in Figure 6a provides anatomical references including the eye, forebrain, midbrain, hindbrain, and spinal cord. New molecules of interest are shown here including a taurine image at m/z 126.01 (Figure 6b) and a histidine image at m/z 156.07 (Figure 6d) as well as previously listed NTs including EP, ACh, GLU, DA/OT, NE, and 5-HT. With this higher spatial resolution, we have the ability to discern anatomical features (e.g., brain, eye, and neural tube) in much more detail than in Figure 5. Specifically, the outline of the eye and the neural tube line are very apparent, as well as differentiation between forebrain, midbrain, and hindbrain. Blank spaces with no NTs detected likely correspond to the otic and pharyngeal cavities.[92] Multiple NTs appear in the organ cavity, including the heart[93] and intestinal area,[94] which have previously been established as sites of NT location in embryonic species. In addition to the previously discussed importance of NTs, histidine is a molecule of interest because it is a precursor to histamine that has important neuroprotective effects,[95] and it has specifically been shown to promote astrocyte migration after cerebral ischemia.[96] Lastly, GABA is an adduct of Na^+ here at m/z 126, which distinguishes the protonated form from the overlapping signal of choline at m/z 104. Choline with a Na^+ adduct would appear at m/z 63 (because it would be doubly charged), making this a clear way to distinguish the two NTs. The corresponding skyline mass spectrum from this MSI run is available in Supporting Information Figure S23.

Continuing with the exploration of difficult to analyze samples, we have also imaged cells with the same approach. Previous examples of single-cell MSI have used only high-resolution instruments[97] or transmission-geometry-based MALDI imaging[36] in this demanding field of research. There are multiple challenges, including achieving a lateral spatial resolution that provides useful cellular information ($\lesssim$5 μm), achieving small enough matrix crystal sizes, and ionizing enough molecules for sufficient detection sensitivity. Previous studies have largely focused on lipids, whereas we have expanded single-cell MSI to small molecules. Figure 7 shows

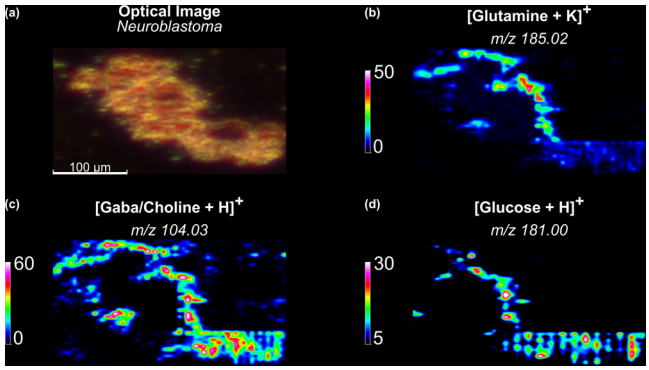

Figure 7. MSI of neuroblastoma cells at 5 μm lateral spatial resolution: (a) confocal optical image depicting the largest grouping of cells, (b) $[GLU + K]^+$ adduct image at m/z 185.02, (c) GABA/choline image at m/z 104.03, and (d) glucose image at m/z 181.00.

neuroblastoma cells that were grown on ITO slides and then imaged at 5 μm. The optical image (Figure 7a) shows the overall cell density within the imaged area, and the molecules imaged are glutamine, GABA, and glucose. The entire rectangular panel was imaged in order to account for potential background signal from the growth media, but no significant signals were observed outside of areas containing a high density of cells.

The use of citrate-capped AuNPs that can be pneumatically sprayed onto tissues extends the analytical capabilities of LDI-MSI to compounds that have been difficult to ionize or must first be derivatized to be ionized and presents a highly time- and cost-effective preparation. While chemical derivatization strategies can target primary amines successfully, extensive synthesis and long preparation times are needed and the cost can be prohibitive at a minimum of $7 per slide for the needed reagents. Even traditional organic matrixes cost at least $1 per slide for reagents and take 2−3 times longer than an AuNP spraying protocol, which costs less than 1000th of a cent per slide. The presented methods enable a broad range of new applications in neuroscience, pharmacology, drug discovery, and pathology.

https://dx.doi.org/10.1021/jasms.0c00156
J. Am. Soc. Mass Spectrom. 2020, 31, 2452−2461

CONCLUSION

In summary, we have demonstrated that AuNPs can effectively ionize neurotransmitters, including molecules that are secondary and tertiary amines and amino acids of interest in the brain. AuNPs can be sprayed pneumatically onto tissue sections for LDI-MS applications, which was demonstrated in rabbit brain, zebrafish embryos, and neuroblastoma cells. Spraying of just one pass of AuNPs was sufficient to obtain high enough NT signal intensities that enabled MSI at a lateral resolution of 5 μm. Furthermore, we have shown the incredible flexibility of AuNPs with regard to sample preparation, tissue storage, and multiple MSI runs of the same AuNP sprayed section.

ASSOCIATED CONTENT

Supporting Information

The Supporting Information is available free of charge on the ACS Publications Web site. The Supporting Information is available free of charge at https://pubs.acs.org/doi/10.1021/jasms.0c00156.

Tables of individual NTs observed species and mass accuracy and MSI on zebrafish tissues, observed species, and mass accuracy and figures of positive ion and representative LDI mass spectra and optical images (PDF)

AUTHOR INFORMATION

Corresponding Author

Katherine A. Stumpo − *Department of Chemistry, University of Scranton, Scranton, Pennsylvania 18510, United States;* orcid.org/0000-0003-3975-8495; Phone: 570-941-7692; Email: katherine.stumpo@scranton.edu; Fax: 570-941-7572

Authors

Nolan McLaughlin − *Department of Chemistry, University of Scranton, Scranton, Pennsylvania 18510, United States*

Tyler M. Bielinski − *Department of Chemistry, University of Scranton, Scranton, Pennsylvania 18510, United States*

Caitlin M. Tressler − *The Russell H. Morgan Department of Radiology and Radiological Science, The Johns Hopkins University School of Medicine, Baltimore, Maryland 21205, United States*

Eric Barton − *The Russell H. Morgan Department of Radiology and Radiological Science, The Johns Hopkins University School of Medicine, Baltimore, Maryland 21205, United States*

Kristine Glunde − *The Russell H. Morgan Department of Radiology and Radiological Science, The Johns Hopkins University School of Medicine, Baltimore, Maryland 21205, United States; The Sidney Kimmel Comprehensive Cancer Center, The Johns Hopkins School of Medicine, Baltimore, Maryland 21205, United States*

Complete contact information is available at: https://pubs.acs.org/10.1021/jasms.0c00156

Notes

The authors declare no competing financial interest.

ACKNOWLEDGMENTS

N.M., T.M.B., and K.A.S. would like to thank the University of Scranton and the Chemistry Department for providing facilities, equipment, and financial support to conduct these experiments. N.M. and K.A.S. would like to thank the University of New Hampshire and Drs. David Ashline and Vernon Reinhold for the use of their Kratos Axima MALDI-TOF MS. K.A.S. would like to thank Dr. Timothy Foley, Alysse Machalek, and Stefan Olsen at the University of Scranton for assistance with the neuroblastoma cell line. The authors would like to thank the Johns Hopkins Applied Imaging Mass Spectrometry (AIMS) Core Facility at the Johns Hopkins University School of Medicine for undertaking the MALDI and LDI imaging in this project.

REFERENCES

(1) Piehowski, P. D.; Zhu, Y.; Bramer, L. M.; Stratton, K. G.; Zhao, R.; Orton, D. J.; Moore, R. J.; Yuan, J.; Mitchell, H. D.; Gao, Y.; Webb-Robertson, B.-J. M.; Dey, S. K.; Kelly, R. T.; Burnum-Johnson, K. E. Automated mass spectrometry imaging of over 2000 proteins from tissue sections at 100-μm spatial resolution. *Nat. Commun.* **2020**, *11*, 8.

(2) Eveque-Mourroux, M. R.; Rocha, B.; Barré, F. P. Y.; Heeren, R. M. A.; Cillero-Pastor, B. Spatially resolved proteomics in osteoarthritis: State of the art and new perspectives. *J. Proteomics* **2020**, *215*, 103637.

(3) Beine, B.; Diehl, H. C.; Meyer, H. E.; Henkel, C. Tissue maldi mass spectrometry imaging (MALDI MSI) of peptides. In *Proteomis in Systems Biology*; Reinders, J., Ed.; Springer New York: New York, NY, 2016; 1394, pp 129−150.

(4) Caprioli, R. M.; Farmer, T. B.; Gile, J. Molecular Imaging of Biological Samples: Localization of Peptides and Proteins Using MALDI-TOF MS. *Anal. Chem.* **1997**, *69*, 4751−4760.

(5) Wang, J.; Wang, C.; Han, X. Enhanced coverage of lipid analysis and imaging by matrix-assisted laser desorption/ionization mass spectrometry via a strategy with an optimized mixture of matrices. *Anal. Chim. Acta* **2018**, *1000*, 155−162.

(6) Angel, P. M.; Spraggins, J. M.; Baldwin, H. S.; Caprioli, R. Enhanced sensitivity for high spatial resolution lipid analysis by negative ion mode matrix assisted laser desorption ionization imaging mass spectrometry. *Anal. Chem.* **2012**, *84*, 1557−1564.

(7) Cologna, S. M. Mass spectrometry imaging of cholesterol. In *Cholesterol Modulation of Protein Function*; Rosenhouse-Dantsker, A., Bukiya, A. N., Eds.; Springer: Cham, 2019; *1115*, pp 155−166.

(8) Sun, C.; Li, T.; Song, X.; Huang, L.; Zang, Q.; Xu, J.; Bi, N.; Jiao, G.; Hao, Y.; Chen, Y.; Zhang, R.; Luo, Z.; Li, X.; Wang, L.; Wang, Z.; Song, Y.; He, J.; Abliz, Z. Spatially resolved metabolomics to discover tumor-associated metabolic alterations. *Proc. Natl. Acad. Sci. U. S. A.* **2019**, *116*, 52−57.

(9) Pareek, V.; Tian, H.; Winograd, N.; Benkovic, S. J. Metabolomics and mass spectrometry imaging reveal channeled de novo purine synthesis in cells. *Science* **2020**, *368*, 283−290.

(10) Dueñas, M. E.; Larson, E. A.; Lee, Y. J. Toward Mass Spectrometry Imaging in the Metabolomics Scale: Increasing Metabolic Coverage Through Multiple On-Tissue Chemical Modifications. *Front. Plant Sci.* **2019**, *10*, 860.

(11) Stoeckli, M.; Staab, D.; Schweitzer, A. Compound and metabolite distribution measured by MALDI mass spectrometric imaging in whole-body tissue sections. *Int. J. Mass Spectrom.* **2007**, *260*, 195−202.

(12) Thomas, S. A.; Jin, Y.; Bunch, J.; Gilmore, I. S. Enhancing classification of mass spectrometry imaging data with deep neural networks. In *2017 IEEE Symposium Series on Computational Intelligence, SSCI 2017 - Proceedings*, Honolulu, HI, Nov 27−Dec 1, 2017; Institute of Electrical and Electronics Engineers Inc; pp 1−8.

(13) Behrmann, J.; Etmann, C.; Boskamp, T.; Casadonte, R.; Kriegsmann, J.; Maaß, P. Deep learning for tumor classification in imaging mass spectrometry | Bioinformatics | Oxford Academic. *Bioinformatics* **2018**, *34*, 1215−1223.

(14) Gusev, A. I.; Wilkinson, W. R.; Proctor, A.; Hercules, D. M. Improvement of signal reproducibility and matrix/comatrix effects in MALDI analysis. *Anal. Chem.* **1995**, *67*, 1034−1041.

(15) Calvano, C. D.; Monopoli, A.; Cataldi, T. R. I.; Palmisano, F. MALDI matrices for low molecular weight compounds: an endless story? *Anal. Bioanal. Chem.* **2018**, *410*, 4015−4038.
(16) Sacks, C.; Stumpo, K. A. Gold Nanoparticles for Enhanced Ionization and Fragmentation of Biomolecules using LDI-MS. *J. Mass Spectrom.* **2018**, *53*, 1070−1077.
(17) McLean, J. A.; Stumpo, K. A.; Russell, D. H. Size-Selected (2−10 nm) Gold Nanoparticles for Matrix Assisted Laser Desorption Ionization of Peptides. *J. Am. Chem. Soc.* **2005**, *127*, 5304−5305.
(18) Basu, S. S.; Regan, M. S.; Randall, E. C.; Abdelmoula, W. M.; Clark, A. R.; Gimenez-Cassina Lopez, B.; Cornett, D. S.; Haase, A.; Santagata, S.; Agar, N. Y. R. Rapid MALDI mass spectrometry imaging for surgical pathology. *npj Precis. Oncol* **2019**, *3*, 1−5.
(19) Santagata, S.; Eberlin, L. S.; Norton, I.; Calligaris, D.; Feldman, D. R.; Ide, J. L.; Liu, X.; Wiley, J. S.; Vestal, M. L.; Ramkissoon, S. H.; Orringer, D. A.; Gill, K. K.; Dunn, I. F.; Dias-Santagata, D.; Ligon, K. L.; Jolesz, F. A.; Golby, A. J.; Cooks, R. G.; Agar, N. Y. R. Intraoperative mass spectrometry mapping of an onco-metabolite to guide brain tumor surgery. *Proc. Natl. Acad. Sci. U. S. A.* **2014**, *111*, 11121−11126.
(20) Eberlin, L. S.; Tibshirani, R. J.; Zhang, J.; Longacre, T. A.; Berry, G. J.; Bingham, D. B.; Norton, J. A.; Zare, R. N.; Poultsides, G. A. Molecular assessment of surgical-resection margins of gastric cancer by mass-spectrometric imaging. *Proc. Natl. Acad. Sci. U. S. A.* **2014**, *111*, 2436−2441.
(21) Buchberger, A. R.; DeLaney, K.; Johnson, J.; Li, L. Mass Spectrometry Imaging: A Review of Emerging Advancements and Future Insights. *Anal. Chem.* **2018**, *90*, 240−265.
(22) Calligaris, D.; Feldman, D. R.; Norton, I.; Olubiyi, O.; Changelian, A. N.; Machaidze, R.; Vestal, M. L.; Laws, E. R.; Dunn, I. F.; Santagata, S.; Agar, N. Y. R. MALDI mass spectrometry imaging analysis of pituitary adenomas for near-real-time tumor delineation. *Proc. Natl. Acad. Sci. U. S. A.* **2015**, *112*, 9978−9983.
(23) Tucker, L. H.; Conde-González, A.; Cobice, D.; Hamm, G. R.; Goodwin, R. J. A.; Campbell, C. J.; Clarke, D. J.; Mackay, C. L. MALDI Matrix Application Utilizing a Modified 3D Printer for Accessible High Resolution Mass Spectrometry Imaging. *Anal. Chem.* **2018**, *90*, 8742−8749.
(24) Iloro, I.; Bueno, A.; Calvo, J.; Urreta, H.; Elortza, F. Langartech: A Custom-Made MALDI Matrix Sprayer for MALDI Imaging Mass Spectrometry. *J. Lab. Autom* **2016**, *21*, 260−267.
(25) Todd, P. J.; Schaaff, T. G.; Chaurand, P.; Caprioli, R. M. Organic ion imaging of biological tissue with secondary ion mass spectrometry and matrix-assisted laser desorption/ionization. *J. Mass Spectrom.* **2001**, *36*, 355−369.
(26) Schuerenberg, M.; Luebbert, C.; Deininger, S.-O.; Ketterlinus, R.; Suckau, D. MALDI tissue imaging: mass spectrometric localization of biomarkers in tissue slices. *Nat. Methods* **2007**, *4*, 462−462.
(27) Yang, J.; Caprioli, R. M. Matrix sublimation/recrystallization for imaging proteins by mass spectrometry at high spatial resolution. *Anal. Chem.* **2011**, *83*, 5728−5734.
(28) Hankin, J. A.; Barkley, R. M.; Murphy, R. C. Sublimation as a method of matrix application for mass spectrometric imaging. *J. Am. Soc. Mass Spectrom.* **2007**, *18*, 1646−1652.
(29) Huizing, L. R. S.; Ellis, S. R.; Beulen, B.W.A.M.M.; Barré, F. P. Y.; Kwant, P. B.; Vreeken, R. J.; Heeren, R. M. A. Development and evaluation of matrix application techniques for high throughput mass spectrometry imaging of tissues in the clinic. *Clin. Mass Spectrom* **2019**, *12*, 7−15.
(30) Anderson, D. M. G.; Floyd, K. A.; Barnes, S.; Clark, J. M.; Clark, J. I.; Mchaourab, H.; Schey, K. L. A method to prevent protein delocalization in imaging mass spectrometry of non-adherent tissues: application to small vertebrate lens imaging. *Anal. Bioanal. Chem.* **2015**, *407*, 2311.
(31) O'Rourke, M. B.; Smith, C. C.; Tse, B. C.; Sutherland, G. T.; Crossett, B.; Padula, M. P. 'What did I do wrong?' An empirical evaluation of sample preparation methodologies in matrix-assisted laser desorption/ionization-mass spectrometry imaging. *Futur. Sci. OA* **2019**, *5*, FSO362.
(32) O'Rourke, M. B.; Djordjevic, S. P.; Padula, M. P. The quest for improved reproducibility in MALDI mass spectrometry. *Mass Spectrom. Rev.* **2018**, *37*, 217−228.
(33) Korte, A. R.; Yandeau-Nelson, M. D.; Nikolau, B. J.; Lee, Y.J. i. Subcellular-level resolution MALDI-MS imaging of maize leaf metabolites by MALDI-linear ion trap-Orbitrap mass spectrometer. *Anal. Bioanal. Chem.* **2015**, *407*, 2301−2309.
(34) Zavalin, A.; Yang, J.; Haase, A.; Holle, A.; Caprioli, R. M. Implementation of a Gaussian Beam Laser and Aspheric Optics for High Spatial Resolution MALDI Imaging MS. *J. Am. Soc. Mass Spectrom.* **2014**, *25*, 1079−1082.
(35) Kompauer, M.; Heiles, S.; Spengler, B. Atmospheric pressure MALDI mass spectrometry imaging of tissues and cells at 1.4-μm lateral resolution. *Nat. Methods* **2017**, *14*, 90−96.
(36) Niehaus, M.; Soltwisch, J.; Belov, M. E.; Dreisewerd, K. Transmission-mode MALDI-2 mass spectrometry imaging of cells and tissues at subcellular resolution. *Nat. Methods* **2019**, *16*, 925−931.
(37) Feenstra, A. D.; Dueñas, M. E.; Lee, Y. J. Five Micron High Resolution MALDI Mass Spectrometry Imaging with Simple, Interchangeable, Multi-Resolution Optical System. *J. Am. Soc. Mass Spectrom.* **2017**, *28*, 434−442.
(38) Shariatgorji, M.; Nilsson, A.; Fridjonsdottir, E.; Vallianatou, T.; Källback, P.; Katan, L.; Sävmarker, J.; Mantas, I.; Zhang, X.; Bezard, E.; Svenningsson, P.; Odell, L. R.; Andrén, P. E. Comprehensive mapping of neurotransmitter networks by MALDI-MS imaging. *Nat. Methods* **2019**, *16*, 1021−1028.
(39) Shariatgorji, M.; Nilsson, A.; Goodwin, R. J. A.; Källback, P.; Schintu, N.; Zhang, X.; Crossman, A. R.; Bezard, E.; Svenningsson, P.; Andren, P. E. Direct targeted quantitative molecular imaging of neurotransmitters in brain tissue sections. *Neuron* **2014**, *84*, 697−707.
(40) Becker, J. S.; Becker, J. S. Imaging of Metals, Metalloids, and Non-metals by Laser Ablation Inductively Coupled Plasma Mass Spectrometry (LA-ICP-MS) in Biological Tissues. In *Mass Spectrometry Imaging*; Sweedler, J. V., Rubakhin, S. S., Eds.; Humana Press: Totowa, NJ, 2010; 656, pp 51−81.
(41) Norris, J. L.; Caprioli, R. M. Analysis of Tissue Specimens by Matrix-Assisted Laser Desorption/Ionization Imaging Mass Spectrometry in Biological and Clinical Research. *Chem. Rev.* **2013**, *113*, 2309−2342.
(42) Palermo, A.; Forsberg, E. M.; Warth, B.; Aisporna, A. E.; Billings, E.; Kuang, E.; Benton, H. P.; Berry, D.; Siuzdak, G. Fluorinated Gold Nanoparticles for Nanostructure Imaging Mass Spectrometry. *ACS Nano* **2018**, *12*, 6938−6948.
(43) Wu, H. P.; Yu, C. J.; Lin, C. Y.; Lin, Y. H.; Tseng, W. L. Gold Nanoparticles as Assisted Matrices for the Detection of Biomolecules in a High-Salt Solution through Laser Desorption/Ionization Mass Spectrometry. *J. Am. Soc. Mass Spectrom.* **2009**, *20*, 875−882.
(44) Su, C. L.; Tseng, W. L. Gold nanoparticles as assisted matrix for determining neutral small carbohydrates through laser desorption/ionization time-of-flight mass spectrometry. *Anal. Chem.* **2007**, *79*, 1626−1633.
(45) Stumpo, K. A.; Russell, D. H. Anion effects on ionization efficiency using gold nanoparticles as matrices for LDI-MS. *J. Phys. Chem. C* **2009**, *113*, 1641−1647.
(46) Dufresne, M.; Thomas, A.; Breault-Turcot, J.; Masson, J. F.; Chaurand, P. Silver-assisted laser desorption ionization for high spatial resolution imaging mass spectrometry of olefins from thin tissue sections. *Anal. Chem.* **2013**, *85*, 3318−3324.
(47) Dufresne, M.; Masson, J.-F.; Chaurand, P. Sodium-Doped Gold-Assisted Laser Desorption Ionization for Enhanced Imaging Mass Spectrometry of Triacylglycerols from Thin Tissue Sections. *Anal. Chem.* **2016**, *88*, 6018−6025.
(48) Wei, J.; Buriak, J. M.; Siuzdak, G. Desorption−ionization mass spectrometry on porous silicon. *Nature* **1999**, *399*, 243−246.
(49) Ren, S. F.; Zhang, L.; Cheng, Z. H.; Guo, Y. L. Immobilized carbon nanotubes as matrix for MALDI-TOF-MS analysis: Applications to neutral small carbohydrates. *J. Am. Soc. Mass Spectrom.* **2005**, *16*, 333−339.

https://dx.doi.org/10.1021/jasms.0c00156
J. Am. Soc. Mass Spectrom. 2020, 31, 2452−2461

(50) Pan, C.; Xu, S.; Hu, L.; Su, X.; Ou, J.; Zou, H.; Guo, Z.; Zhang, Y.; Guo, B. Using Oxidized Carbon Nanotubes as Matrix for Analysis of Small Molecules by MALDI-TOF MS. *J. Am. Soc. Mass Spectrom.* **2005**, *16*, 883−892.
(51) Shahnawaz Khan, M.; Bhaisare, M. L.; Pandey, S.; Talib, A.; Wu, S. M.; Kailasa, S. K.; Wu, H. F. Exploring the ability of water soluble carbon dots as matrix for detecting neurological disorders using MALDI-TOF MS. *Int. J. Mass Spectrom.* **2015**, *393*, 25−33.
(52) Castellana, E. T.; Russell, D. H. Tailoring Nanoparticle Surface Chemistry to Enhance Laser Desorption Ionization of Peptides and Proteins. *Nano Lett.* **2007**, *7*, 3023−3025.
(53) Karas, M.; Hillenkamp, F. Laser desorption ionization of proteins with molecular masses exceeding 10,000 Da. *Anal. Chem.* **1988**, *60*, 2299−2301.
(54) Fernández, J. A.; Ochoa, B.; Fresnedo, O.; Giralt, M. T.; Rodríguez-Puertas, R. Matrix-assisted laser desorption ionization imaging mass spectrometry in lipidomics. *Anal. Bioanal. Chem.* **2011**, *401*, 29−51.
(55) Abdelhamid, H. N.; Wu, H. F. Gold nanoparticles assisted laser desorption/ionization mass spectrometry and applications: from simple molecules to intact cells. *Anal. Bioanal. Chem.* **2016**, *408*, 4485−4502.
(56) Nizioł, J.; Ossoliński, K.; Ossoliński, T.; Ossolińska, A.; Bonifay, V.; Sekuła, J.; Dobrowolski, Z.; Sunner, J.; Beech, I.; Ruman, T. Surface-Transfer Mass Spectrometry Imaging of Renal Tissue on Gold Nanoparticle Enhanced Target. *Anal. Chem.* **2016**, *88*, 7365−7371.
(57) Misiorek, M.; Sekuła, J.; Ruman, T. Mass Spectrometry Imaging of low Molecular Weight Compounds in Garlic (*Allium sativum* L.) with Gold Nanoparticle Enhanced Target. *Phytochem. Anal.* **2017**, *28*, 479−486.
(58) Ràfols, P.; Vilalta, D.; Torres, S.; Calavia, R.; Heijs, B.; McDonnell, L. A.; Brezmes, J.; del Castillo, E.; Yanes, O.; Ramírez, N.; Correig, X. Assessing the potential of sputtered gold nanolayers in mass spectrometry imaging for metabolomics applications. *PLoS One* **2018**, *13* (12), e0208908.
(59) Hansen, R. L.; Dueñas, M. E.; Lee, Y. J. Sputter-Coated Metal Screening for Small Molecule Analysis and High-Spatial Resolution Imaging in Laser Desorption Ionization Mass Spectrometry. *J. Am. Soc. Mass Spectrom.* **2019**, *30*, 299−308.
(60) Yang, E.; Fournelle, F.; Chaurand, P. Silver spray deposition for AgLDI imaging MS of cholesterol and other olefins on thin tissue sections. *J. Mass Spectrom.* **2020**, *55* (4), e4428.
(61) Ràfols, P.; Castillo, E. d.; Yanes, O.; Brezmes, J.; Correig, X. Novel automated workflow for spectral alignment and mass calibration in MS imaging using a sputtered Ag nanolayer. *Anal. Chim. Acta* **2018**, *1022*, 61−69.
(62) Ščupáková, K.; Balluff, B.; Tressler, C.; Adelaja, T.; Heeren, R. M. A.; Glunde, K.; Ertaylan, G. Cellular resolution in clinical MALDI mass spectrometry imaging: The latest advancements and current challenges. *Clin. Chem. Lab. Med.* **2020**, *58*, 914.
(63) Trim, P. J.; Snel, M. F. Small molecule MALDI MS imaging: Current technologies and future challenges. *Methods* **2016**, *104*, 127−141.
(64) Källback, P.; Nilsson, A.; Shariatgorji, M.; Andrén, P. E. MsIQuant - Quantitation Software for Mass Spectrometry Imaging Enabling Fast Access, Visualization, and Analysis of Large Data Sets. *Anal. Chem.* **2016**, *88*, 4346−4353.
(65) Bemis, K. D.; Harry, A.; Eberlin, L. S.; Ferreira, C.; van de Ven, S. M.; Mallick, P.; Stolowitz, M.; Vitek, O. Cardinal: an R package for statistical analysis of mass spectrometry-based imaging experiments: Fig. 1. *Bioinformatics* **2015**, *31*, 2418−2420.
(66) *Neurodegeneration*; Manfredi, G., Kawamata, H., Eds.; Humana Press: Totowa, NJ, 2011; *793*, p 6.
(67) Golabi, P.; Elsheikh, E.; Karrar, A.; Estep, J. M.; Younossi, I.; Stepanova, M.; Gerber, L.; Younossi, Z. M. The levels of monoamine neurotransmitters and measures of mental and emotional health in HCV patients treated with ledipasvir (LDV) and sofosbuvir (SOF) with or without ribavirin (RBV). *Medicine (Philadelphia, PA, U. S.)* **2016**, *95*, e5066.
(68) Janik, P.; Kalbarczyk, A.; Gutowicz, M.; Barańczyk-Kuźma, A.; Kwieciński, H. The analysis of selected neurotransmitter concentrations in serum of patients with Tourette syndrome. *Neurol. Neurochir. Pol.* **2010**, *44*, 251−9.
(69) Zheng, X.; Zhang, J.; Wei, H.; Chen, H.; Tian, Y.; Zhang, J. Determination of Dopamine in Cerebrospinal Fluid by MALDI-TOF Mass Spectrometry with a Functionalized Graphene Oxide Matrix. *Anal. Lett.* **2016**, *49*, 1847−1861.
(70) Bucknall, M.; Fung, K. Y. C.; Duncan, M. W. Practical quantitative biomedical applications of MALDI-TOF mass spectrometry. *J. Am. Soc. Mass Spectrom.* **2002**, *13*, 1015−1027.
(71) Suominen, T.; Uutela, P.; Ketola, R. A.; Bergquist, J.; Hillered, L.; Finel, M.; Zhang, H.; Laakso, A.; Kostiainen, R. Determination of Serotonin and Dopamine Metabolites in Human Brain Microdialysis and Cerebrospinal Fluid Samples by UPLC-MS/MS: Discovery of Intact Glucuronide and Sulfate Conjugates. *PLoS One* **2013**, *8*, e68007.
(72) Najmanová, V.; Rambousek, L.; Syslová, K.; Bubeníková, V.; Šlamberová, R.; Valeš, K.; Kačer, P. LC-ESI-MS-MS Method for Monitoring Dopamine, Serotonin and Their Metabolites in Brain Tissue. *Chromatographia* **2011**, *73*, 143−149.
(73) Jensen, J. E.; Frederick, B. d.; Renshaw, P. F. Grey and white matter GABA level differences in the human brain using two-dimensional, J-resolved spectroscopic imaging. *NMR Biomed.* **2005**, *18*, 570−576.
(74) Choi, I. Y.; Lee, S. P.; Merkle, H.; Shen, J. In vivo detection of gray and white matter differences in GABA concentration in the human brain. *NeuroImage* **2006**, *33*, 85−93.
(75) Reader, T. A.; Masse, P.; Champlain, J. d. The intracortical distribution of norepinephrine, dopamine and serotonin in the cerebral cortex of the cat. *Brain Res.* **1979**, *177*, 499−513.
(76) Ciarmiello, A.; Cannella, M.; Lastoria, S.; Simonelli, M.; Frati, L.; Rubinsztein, D. C.; Squitieri, F. Brain white-matter volume loss and glucose hypometabolism precede the clinical symptoms of Huntington's disease. *J. Nucl. Med.* **2006**, *47* (2), 215−222.
(77) Haghshomar, M.; Rahmani, F.; Hadi Aarabi, M.; Shahjouei, S.; Sobhani, S.; Rahmani, M. White Matter Changes Correlates of Peripheral Neuroinflammation in Patients with Parkinson's Disease. *Neuroscience* **2019**, *403*, 70−78.
(78) Howe, K.; Clark, M. D.; Torroja, C. F.; Torrance, J.; Berthelot, C.; Muffato, M.; Collins, J. E.; Humphray, S.; McLaren, K.; Matthews, L.; McLaren, S.; Sealy, I.; Caccamo, M.; Churcher, C.; Scott, C.; Barrett, J. C.; Koch, R.; Rauch, G.-J.; White, S.; Chow, W.; Kilian, B.; Quintais, L. T.; Guerra-Assuncao, J. A.; Zhou, Y.; Gu, Y.; Yen, J.; Vogel, J.-H.; Eyre, T.; Redmond, S.; Banerjee, R.; Chi, J.; Fu, B.; Langley, E.; Maguire, S. F.; Laird, G. K.; Lloyd, D.; Kenyon, E.; Donaldson, S.; Sehra, H.; Almeida-King, J.; Loveland, J.; Trevanion, S.; Jones, M.; Quail, M.; Willey, D.; Hunt, A.; Burton, J.; Sims, S.; McLay, K.; Plumb, B.; Davis, J.; Clee, C.; Oliver, K.; Clark, R.; Riddle, C.; Elliott, D.; Threadgold, G.; Harden, G.; Ware, D.; Begum, S.; Mortimore, B.; Kerry, G.; Heath, P.; Phillimore, B.; Tracey, A.; Corby, N.; Dunn, M.; Johnson, C.; Wood, J.; Clark, S.; Pelan, S.; Griffiths, G.; Smith, M.; Glithero, R.; Howden, P.; Barker, N.; Lloyd, C.; Stevens, C.; Harley, J.; Holt, K.; Panagiotidis, G.; Lovell, J.; Beasley, H.; Henderson, C.; Gordon, D.; Auger, K.; Wright, D.; Collins, J.; Raisen, C.; Dyer, L.; Leung, K.; Robertson, L.; Ambridge, K.; Leongamornlert, D.; McGuire, S.; Gilderthorp, R.; Griffiths, C.; Manthravadi, D.; Nichol, S.; Barker, G.; Whitehead, S.; Kay, M.; Brown, J.; Murnane, C.; Gray, E.; Humphries, M.; Sycamore, N.; Barker, D.; Saunders, D.; Wallis, J.; Babbage, A.; Hammond, S.; Mashreghi-Mohammadi, M.; Barr, L.; Martin, S.; Wray, P.; Ellington, A.; Matthews, N.; Ellwood, M.; Woodmansey, R.; Clark, G.; Cooper, J. D.; Tromans, A.; Grafham, D.; Skuce, C.; Pandian, R.; Andrews, R.; Harrison, E.; Kimberley, A.; Garnett, J.; Fosker, N.; Hall, R.; Garner, P.; Kelly, D.; Bird, C.; Palmer, S.; Gehring, I.; Berger, A.; Dooley, C. M.; Ersan-Urun, Z.; Eser, C.; Geiger, H.; Geisler, M.; Karotki, L.; Kirn, A.; Konantz, J.; Konantz, M.; Oberlander, M.; Rudolph-Geiger, S.; Teucke, M.; Lanz, C.; Raddatz, G.; Osoegawa, K.; Zhu, B.; Rapp, A.; Widaa, S.; Langford, C.; Yang, F.; Schuster, S. C.; Carter, N. P.;

https://dx.doi.org/10.1021/jasms.0c00156
J. Am. Soc. Mass Spectrom. 2020, 31, 2452−2461

Harrow, J.; Ning, Z.; Herrero, J.; Searle, S. M. J.; Enright, A.; Geisler, R.; Plasterk, R. H. A.; Lee, C.; Westerfield, M.; de Jong, P. J.; Zon, L. I.; Postlethwait, J. H.; Nusslein-Volhard, C.; Hubbard, T. J. P.; Crollius, H. R.; Rogers, J.; Stemple, D. L. The zebrafish reference genome sequence and its relationship to the human genome. *Nature* **2013**, *496*, 498−503.
(79) Wood, P. B.; Ledbetter, C. R.; Glabus, M. F.; Broadwell, L. K.; Patterson, J. C. Hippocampal Metabolite Abnormalities in Fibromyalgia: Correlation With Clinical Features. *J. Pain* **2009**, *10*, 47−52.
(80) Murphy, R. C.; Axelsen, P. H. Mass spectrometric analysis of long-chain lipids. *Mass Spectrom. Rev.* **2011**, *30*, 579−599.
(81) Van Hove, E. R. A.; Blackwell, T. R.; Klinkert, I.; Eijkel, G. B.; Heeren, R. M. A.; Glunde, K. Multimodal mass spectrometric imaging of small molecules reveals distinct spatio-molecular signatures in differentially metastatic breast tumor models. *Cancer Res.* **2010**, *70*, 9012−9021.
(82) Driever, W.; Stemple, D.; Schier, A.; Solnica-Krezel, L. Zebrafish: genetic tools for studying vertebrate development. *Trends Genet.* **1994**, *10*, 152−159.
(83) Panula, P.; Sallinen, V.; Sundvik, M.; Kolehmainen, J.; Torkko, V.; Tiittula, A.; Moshnyakov, M.; Podlasz, P. Modulatory neurotransmitter systems and behavior: Towards zebrafish models of neurodegenerative diseases. *Zebrafish* **2006**, *3*, 235−247.
(84) Saleem, S.; Kannan, R. R. Zebrafish: an emerging real-time model system to study Alzheimer's disease and neurospecific drug discovery. *Cell Death Discov* **2018**, *4*, 45.
(85) Lieschke, G. J.; Currie, P. D. Animal models of human disease: Zebrafish swim into view. *Nat. Rev. Genet.* **2007**, *8*, 353−367.
(86) Horzmann, K. A.; Freeman, J. L. Zebrafish get connected: Investigating neurotransmission targets and alterations in chemical toxicity. *Toxics* **2016**, *4*, 19.
(87) Hill, A. J.; Teraoka, H.; Heideman, W.; Peterson, R. E. Zebrafish as a model vertebrate for investigating chemical toxicity. *Toxicol. Sci.* **2005**, *86*, 6−19.
(88) Raible, D. W.; Wood, A.; Hodsdon, W.; Henion, P. D.; Weston, J. A.; Eisen, J. S. Segregation and early dispersal of neural crest cells in the embryonic zebrafish. *Dev. Dyn.* **1992**, *195*, 29−42.
(89) Steven, R. T.; Bunch, J. Repeat MALDI MS imaging of a single tissue section using multiple matrices and tissue washes. *Anal. Bioanal. Chem.* **2013**, *405*, 4719−4728.
(90) Goodwin, R. J. A. Sample preparation for mass spectrometry imaging: Small mistakes can lead to big consequences. *J. Proteomics* **2012**, *75*, 4893−4911.
(91) Swales, J. G.; Hamm, G.; Clench, M. R.; Goodwin, R. J. A. Mass spectrometry imaging and its application in pharmaceutical research and development: A concise review. *Int. J. Mass Spectrom.* **2019**, *437*, 99−112.
(92) Cheng, K.; Copper, J. E. Penn State Bio-Atlas. http://zfatlas.psu.edu (accessed 04/15/2020).
(93) Vargas, R. A. Effects of GABA, Neural Regulation, and Intrinsic Cardiac Factors on Heart Rate Variability in Zebrafish Larvae. *Zebrafish* **2017**, *14*, 106−117.
(94) Njagi, J.; Ball, M.; Best, M.; Wallace, K. N.; Andreescu, S. Electrochemical Quantification of Serotonin in the Live Embryonic Zebrafish Intestine. *Anal. Chem.* **2010**, *82*, 1822−1830.
(95) Bae, O. N.; Majid, A. Role of histidine/histamine in carnosine-induced neuroprotection during ischemic brain damage. *Brain Res.* **2013**, *1527*, 246−254.
(96) Liao, R. J.; Jiang, L.; Wang, R. R.; Zhao, H. W.; Chen, Y.; Li, Y.; Wang, L.; Jie, L. Y.; Zhou, Y. D.; Zhang, X. N.; Chen, Z.; Hu, W. W. Histidine provides long-term neuroprotection after cerebral ischemia through promoting astrocyte migration. *Sci. Rep.* **2015**, *5*, 1−14.
(97) Gilmore, I. S.; Heiles, S.; Pieterse, C. L. Metabolic Imaging at the Single-Cell Scale: Recent Advances in Mass Spectrometry Imaging. *Annu. Rev. Anal. Chem.* **2019**, *12*, 201−224.

https://dx.doi.org/10.1021/jasms.0c00156
J. Am. Soc. Mass Spectrom. 2020, 31, 2452−2461